Arch. Metall. Mater. **65** (2020), 4, 1311-1315

DOI: 10.24425/amm.2020.133691

SEONGI LEE[1], KWANGMIN LEE[1*]

MICROSTRUCTURE AND MECHANICAL PROPERTIES OF EQUIATOMIC AND NON-EQUIATOMIC TiMoTaNbV HIGH ENTROPY ALLOYS PREPARED USING VACUUM ARC REMELTING

This study investigates the microstructures and the mechanical properties of equiatomic $Ti_{20}Mo_{20}Ta_{20}Nb_{20}V_{20}$ and non-equiatomic $Ti_{40}Mo_{15}Ta_{15}Nb_{15}V_{15}$ and $Ti_{60}Mo_{10}Ta_{10}Nb_{10}V_{10}$ HEAs using X-ray diffraction (XRD) analysis, field emission scanning electron microscope (FE-SEM), and micro-Vickers hardness test. The specimens were fabricated using the vacuum arc remelting (VAR) process and homogenized at a temperature of 1300°C for 4 h in a vacuum atmosphere. The determined thermodynamic parameters, $\Omega \geq 1.1$, $\delta \leq 6.6\%$, and VEC < 6.87, suggested that the HEAs consisted of BCC solid solutions. XRD patterns of all the HEAs displayed single BCC phases. The difference in the solidification rate led to the micro-segregation associated with the elements Ta and Mo enriched in the dendrite arms and the elements V and Ti in the inter-dendritic regions. The HEA specimens showed a decrease in hardness with higher concentration of Ti element because the intrinsic hardness of Ti is lower as compared to the intrinsic hardness of Nb and Mo.

Keywords: High Entropy Alloy, TiMoTaNbV, Vacuum Arc Remelting, BCC Phase, Micro-segregation

1. Introduction

High entropy alloys (HEAs) with equiatomic or near equiatomic compositions (five or more principal elements) have attracted significant attention because of their high configurational entropy [1,2]. Yeh et al. proposed that the four core effects, namely the high entropy effect, the sluggish diffusion effect, the severe lattice distortion effect, and the cocktail effect, provide superior physical and mechanical properties [2]. The HEAs consisting of elements from Group IV (Ti, Zr, and Hf), Group V (V, Nb, and Ta), and Group VI (Cr, Mo, and W) could be the potential candidates as the metallic biomaterials in the cardiovascular stents. It is known that these elements are remarkably biocompatible with the human body.

L605 (ASTM F90) and MP35N (ASTM F562) alloys are the representative cardiovascular stents, because of their low profiles, high expandability ratio, and high radial hoop strength [3]. A balance between strength and ductility is essential in the materials being used in the stents to achieve smaller strut sizes and sufficient strength. HEAs are the suitable candidates to achieve the requisite strength-ductility balance in the stents owing to the formation of single phase solid solutions.

The refractory HEAs were focused on improving the high temperature strength in addition to solving the issue of lack of ductility at low temperatures [4-6]. Senkov et al. [7] researched high temperature structural materials to replace the Ni-based superalloys, and proposed the refractory HEAs. Recently, Yao et al. [8] reported improved mechanical properties of refractory MoNbTaTiV HEA with CALPHAD modeling.

The constituent elements of the refractory HEAs are similar to the constituent elements of the HEAs used in biomedical applications. Increasing an amount of Ti element up to non-equiatomic composition of HEA can give us an opportunity in obtaining unique strength-ductility balance for metallic biomaterials. Therefore, in this study, the various thermodynamic parameters, the microstructures, and the mechanical properties of equiatomic and non-equiatomic TiMoTaNbV HEAs were investigated by using the vacuum arc remelting (VAR) process.

2. Experimental

In this study, $Ti_{20}Mo_{20}Ta_{20}Nb_{20}V_{20}$, $Ti_{40}Mo_{15}Ta_{15}Nb_{15}V_{15}$ and $Ti_{60}Mo_{10}Ta_{10}Nb_{10}V_{10}$ HEAs were fabricated using the vacuum arc remelting (VAR, ACE VACUUM, AVA-1500, Korea). Commercially pure Ti chips (ASTM CP Grade II), Mo bars (99.8 wt.%), Ta chips (99.9 wt.%), Nb chips (99.9 wt.%), and V sheets (99.9 wt.%) were arc melted in a water-cooled

[1] SCHOOL OF MATERIALS SCIENCE & ENGINEERING, CHONNAM NATIONAL UNIVERSITY, GWANGJU 61186, REPUBLIC OF KOREA

* Corresponding author: kmlee@jnu.ac.kr

© 2020. The Author(s). This is an open-access article distributed under the terms of the Creative Commons Attribution-NonCommercial License (CC BY-NC 4.0, https://creativecommons.org/licenses/by-nc/4.0/deed.en which permits the use, redistribution of the material in any medium or format, transforming and building upon the material, provided that the article is properly cited, the use is noncommercial, and no modifications or adaptations are made.

copper hearth containing a tungsten electrode. The ingots were flipped subsequently and re-melted five times in an argon rich atmosphere to ensure chemical homogeneity. All the cast ingots were then homogenized at 1300°C for 4 h. The actual chemical compositions (at%) of TiMoTaNbV HEAs analyzed using EDS attached FE-SEM are given in Table 1.

TABLE 1

Actual chemical compositions (at%) of TiMoTaNbV HEAs analyzed using EDS attached FE-SEM

Alloy	Ti	Mo	Ta	Nb	V	Total
$Ti_{20}Mo_{20}Ta_{20}Nb_{20}V_{20}$	21.5	19.7	20.6	16.5	21.7	100.00
$Ti_{40}Mo_{15}Ta_{15}Nb_{15}V_{15}$	44.6	15.9	12.5	11.5	15.4	100.00
$Ti_{60}Mo_{10}Ta_{10}Nb_{10}V_{15}$	62.8	8.6	10.7	8.3	9.6	100.00

The phase constitutions of the alloys were examined using X-ray diffraction (XRD, PANalytical, X' Pert pro, Netherland) analysis. It used the Cu-Kα radiation over a 2θ range from 10°-90° at an accelerating voltage of 40 kV, a current of 250 mA, and a scanning speed of 2°/min. Field emission scanning electron microscope (FE-SEM, Gemini 500, ZEISS, Germany) in conjunction with energy dispersive X-ray spectroscopy (EDS) were used to characterize the microstructures of HEAs. The hardness of HEAs was measured using a micro-Vickers hardness tester (Innovatst Nova 130, Europe) with a load of approximately 10 N load for a holding time of 15 s. Ten random measurements were made on the polished surface of each sample to obtain an average value.

3. Results and discussion

Thermodynamic criteria were proposed to predict the stable phases of the multi-principal element alloys (MPEAs). The parameters include the enthalpy of mixing (ΔH_{mix}), the entropy of mixing (ΔS_{mix}), and the Ω-parameter [9]. In addition, the atomic size difference (δ) [10] and the valance electron concentration (VEC) [11] were used to predict the formation of a solid solution in the MPEAs. Equations for these terms are expressed as:

$$\Delta H_{mix} = \sum_{i=1, i\neq j} \Omega_{ij} c_i c_j \tag{1}$$

where, $\Omega_{ij} = 4\Delta H_{mix}^{AB}$ is the regular solution interaction parameter between the i^{th} and the j^{th} elements, c_i and c_j are the atomic percentages of the i^{th} and the j^{th} components, respectively, and ΔH_{mix}^{AB} is the enthalpy of mixing of binary alloys.

$$\Delta S_{mix} = -R\sum_{i=1}^{n}(c_i \ln c_i) \tag{2}$$

where c_i is the atomic percentage of the i^{th} component and R (8.314 J/k·mol) is the gas constant.

$$\Omega = \frac{T_m \Delta S_{mix}}{|\Delta H_{mix}|} \tag{3}$$

where, c_i is the atomic percentage of the i^{th} component and $(T_m)_i$ is the melting point of the i^{th} component of the alloy.

$$\delta = 100\sqrt{\sum_{i=1}^{n} c_i \left(1 - \frac{r_i}{\bar{r}}\right)^2} \tag{4}$$

c_i is the atomic percentage of the i^{th} component, $\bar{r} = \sum_{i=1}^{n} c_i r_i$ is the average atomic radius, and r_i is the atomic radius.

$$VEC = \sum_{i=1}^{n} c_i (VEC)_i \tag{5}$$

where c_i is the atomic percentage of the i^{th} component and VEC_i is the VEC for the i^{th} element.

Table 2 shows the various thermodynamic parameters calculated using Eqs. (1), (2), (3), (4), and (5) to predict the formation of the solid solution phase in the TiMoTaNbV HEA alloys. The values of Ω-parameter, the δ, and the VEC for equiatomic HEA $Ti_{20}Mo_{20}Ta_{20}Nb_{20}V_{20}$ were 13.6, 4.03%, and 5, for non-equiatomic HEA $Ti_{40}Mo_{15}Ta_{15}Nb_{15}V_{15}$ were 16.18, 3.57%, and 4.75, and for non-equiatomic HEA $Ti_{60}Mo_{10}Ta_{10}Nb_{10}V_{10}$ were 20.13, 2.81%, and 4.5, respectively. The obtained values of the Ω-parameter and the δ for the HEAs were found to be $\Omega \geq 1.1$ and $\delta \leq 6.6\%$ [9], suggesting an effective formation of solid solutions. All the VEC values were located at VEC < 6.87 [11], indicating the formation of BCC solid solutions.

TABLE 2

Thermodynamic parameters (δ, ΔH_{mix}, ΔS_{mix}, Ω, and VEC) used to predict the formation of solid solution phase in the TiMoTaNbV HEA alloys

Alloy	δ (%)	ΔH_{mix} (kJ/mol)	ΔS_{mix} (J/K·mol)	Ω	VEC
$Ti_{20}Mo_{20}Ta_{20}Nb_{20}V_{20}$	4.03	–2.56	13.36	13.6	5
$Ti_{40}Mo_{15}Ta_{15}Nb_{15}V_{15}$	3.57	–1.89	12.51	16.18	4.75
$Ti_{60}Mo_{10}Ta_{10}Nb_{10}V_{10}$	2.81	–1.24	10.97	20.13	4.5

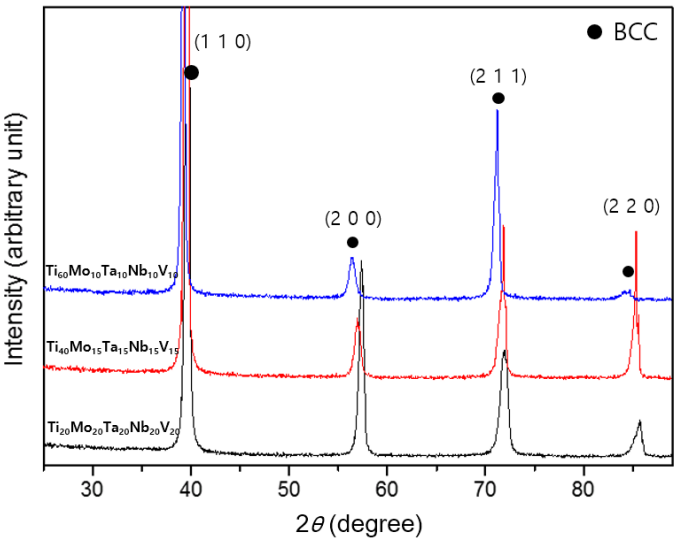

Fig. 1. XRD patterns of the equiatomic $Ti_{20}Mo_{20}Ta_{20}Nb_{20}V_{20}$ and the non-equiatomic $Ti_{40}Mo_{15}Ta_{15}Nb_{15}V_{15}$ and $Ti_{60}Mo_{10}Ta_{10}Nb_{10}V_{10}$ HEAs

Fig. 1 shows the XRD patterns of the equiatomic HEA $Ti_{20}Mo_{20}Ta_{20}Nb_{20}V_{20}$ and the non-equiatomic $Ti_{40}Mo_{15}Ta_{15}Nb_{15}V_{15}$ and $Ti_{60}Mo_{10}Ta_{10}Nb_{10}V_{10}$ HEAs. All the samples showed that the four main X-ray peaks on the planes (110), (200), (211), and (220) corresponded to a single BCC phase. In addition, the XRD patterns were shifted slightly to the right because the high alloying elements led to a crystal lattice strain. The lattice parameter (a_{mix}) of the alloy can be estimated using the rule of mixtures, the Vegard's law [12]. The a_{mix} parameter is expressed as:

$$a_{mix} = \sum c_i a_i \tag{6}$$

where, c_i is the atomic percentage of the i^{th} component and a_i is the lattice parameter of the i^{th} element.

In the (110), (200), and (211) planes, the calculated lattice parameters corresponded to 3.211, 3.228, and 3.244 Å, and the experimental lattice parameters corresponded to 3.214, 3.225, and 3.241 Å for the $Ti_{20}Mo_{20}Ta_{20}Nb_{20}V_{20}$, $Ti_{40}Mo_{15}Ta_{15}Nb_{15}V_{15}$, and $Ti_{60}Mo_{10}Ta_{10}Nb_{10}V_{10}$ HEAs, respectively. The lattice parameters of the HEAs calculated using the rule of mixtures were reasonably similar to those calculated using the XRD analysis.

Fig. 2 shows the backscattered-electron (BSE) SEM images and a series of EDS mapping of elements Ti, Mo, Ta, Nb, and V, which are the alloying elements for the $Ti_{20}Mo_{20}Ta_{20}Nb_{20}V_{20}$, $Ti_{40}Mo_{15}Ta_{15}Nb_{15}V_{15}$, and $Ti_{60}Mo_{10}Ta_{10}Nb_{10}V_{10}$ HEAs. As shown in the BSE images in Figs. 2(a) and (b), representative dendritic microstructures were formed because of the constitutional micro-segregation during the non-equilibrium solidifica-

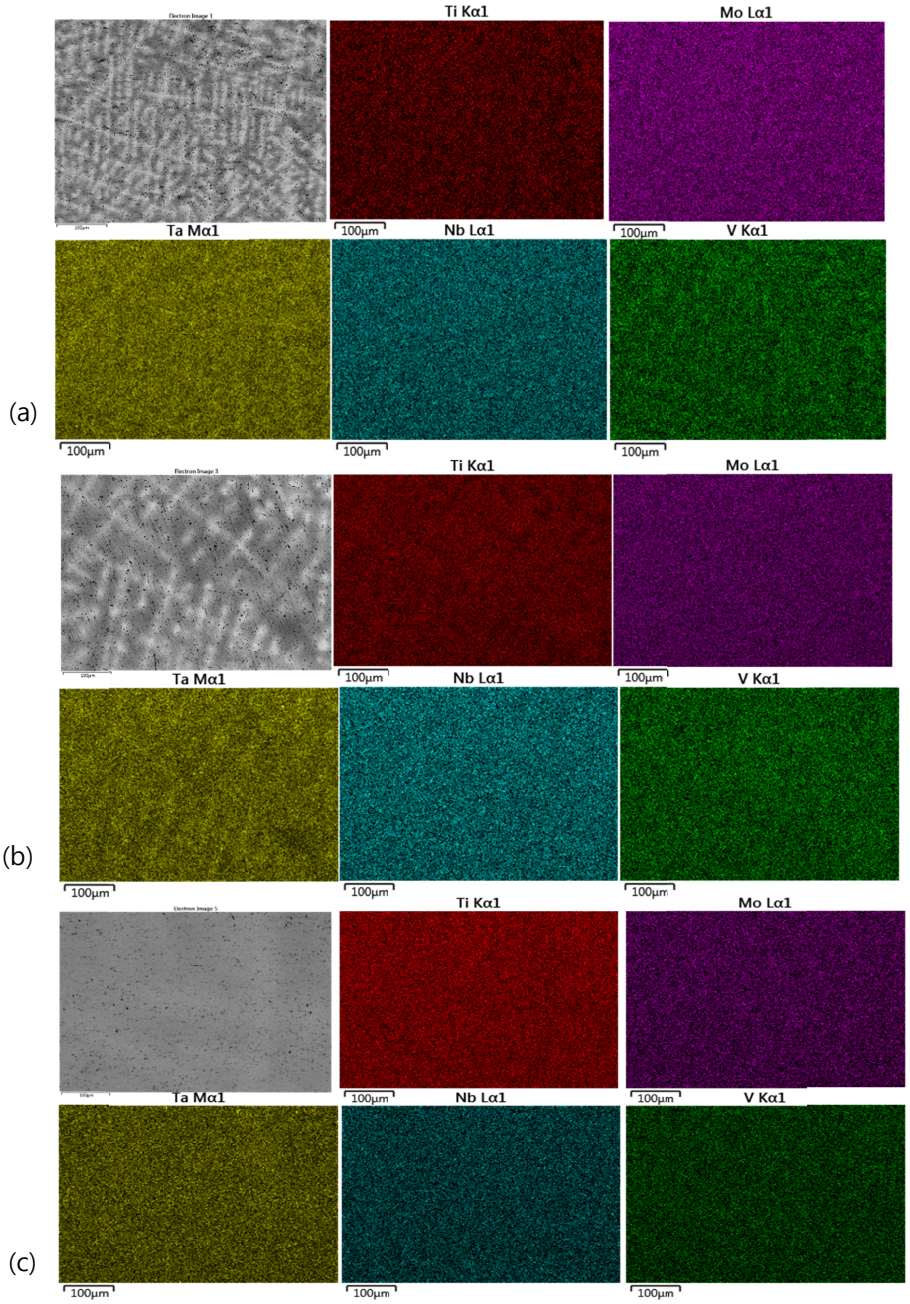

Fig. 2. Backscattered-electron (BSE) SEM images and the EDS mapping of the alloying elements Ti, Mo, Ta, Nb, and V for the TiMoTaNbV HEAs: (a) $Ti_{20}Mo_{20}Ta_{20}Nb_{20}V_{20}$ HEA, (b) $Ti_{40}Mo_{15}Ta_{15}Nb_{15}V_{15}$ HEA, (c) $Ti_{60}Mo_{10}Ta_{10}Nb_{10}V_{10}$ HEA

tion. The dendrite arms exhibiting a light contrast were rich in the element Ta because of its much heavier atomic weight (180.95) compared to the others, whereas the elements Mo, Nb, V and Ti were not distinguishable in the EDS mapping. In contrast, Fig. 2(c) revealed that micro-segregation of the non-equiatomic $Ti_{60}Mo_{10}Ta_{10}Nb_{10}V_{10}$ HEAs appeared to decrease remarkably, because small amount with high melting points of refractory elements such as Mo, Ta, and Nb could cause to decrease the formation of dendrite and inter-dendrite regions during non-equilibrium solidification.

The average elemental composition in the dendrite arms (C_{dr}) and the inter-dendrite regions (C_{idr}) for the HEAs through the EDS analyses is listed in Table 3. Generally the partition coefficient ($k = C_{dr} / C_{idr}$) [7] is usually used to quantitatively estimate the micro-segregation of the alloying elements. The values of k for elements Ta and Mo in the equiatomic $Ti_{20}Mo_{20}Ta_{20}Nb_{20}V_{20}$ HEA were higher than the values of k for elements Ti and V in the other HEAs. The elemental distribution can be observed in the values of k for elements between the dendrite and the inter-dendrite regions in the Table 3. The dendrite arms were rich in the elements Ta and Mo, whereas the inter-dendritic regions were rich in the elements V and Ti. Elements Ta and Mo were first solidified in the dendrite arm owing to their higher melting temperature in the HEAs. Elements Ti and V solidified later and appeared to be in the inter-dendrite regions owing to their lower melting temperature [7]. Nb at approximately $k = 1$ was commonly found in the dendrite arm and the inter-dendrite regions of theses HEAs. The partition coefficient of each alloying element in the non-equiatomic $Ti_{60}Mo_{10}Ta_{10}Nb_{10}V_{10}$ HEA was consistent with the uniform elemental distribution as discussed in Fig. 2(c).

TABLE 3

Average composition of dendrite arms (C_{dr}) and inter-dendrite regions (C_{idr}) and the partition coefficient of k for the equiatomic $Ti_{20}Mo_{20}Ta_{20}Nb_{20}V_{20}$ HEA and the non-equiatomic $Ti_{40}Mo_{15}Ta_{15}Nb_{15}V_{15}$ and $Ti_{60}Mo_{10}Ta_{10}Nb_{10}V_{10}$ HEAs

Alloy	Concentrations (at%)	Ti	Mo	Ta	Nb	V
$Ti_{20}Mo_{20}Ta_{20}Nb_{20}V_{20}$	C_{dr}	17.9	22.4	24.6	16.7	18.2
	C_{idr}	24.9	17.6	16.9	16.2	24.3
	$k = C_{dr}/C_{idr}$	0.72	1.27	1.46	1.03	0.75
$Ti_{40}Mo_{15}Ta_{15}Nb_{15}V_{15}$	C_{dr}	42.3	17.6	14.9	11.8	13.3
	C_{idr}	48.2	18.9	10.3	11.3	16.2
	$k = C_{dr}/C_{idr}$	0.88	0.93	1.45	1.04	0.82
$Ti_{60}Mo_{10}Ta_{10}Nb_{10}V_{15}$	C_{dr}	60.8	9.1	11.9	8.5	9.7
	C_{idr}	63.8	8.2	10.1	8.3	9.7
	$k = C_{dr}/C_{idr}$	0.95	1.11	1.18	1.02	1.01

Fig. 3 shows Vickers hardness for all the HEA specimens. For equiatomic $Ti_{20}Mo_{20}Ta_{20}Nb_{20}V_{20}$, and non-equiatomic $Ti_{40}Mo_{15}Ta_{15}Nb_{15}V_{15}$ and $Ti_{60}Mo_{10}Ta_{10}Nb_{10}V_{10}$ HEAs, the average hardness values were 446.2 Hv, 423.4 Hv, and 398.2 Hv, respectively. The non-equiatomic HEAs with higher concentration of element Ti displayed a decrease in the hardness because the intrinsic hardness of Ti is lower as compared to the intrinsic hardness of Nb and Mo. In addition, the micro-Vickers hardness values for the other refractory HEAs were referred for comparison [8,13-17].

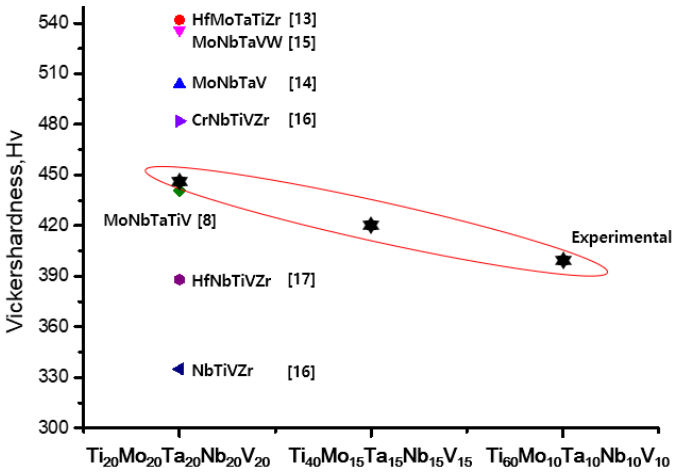

Fig. 3. Micro-Vickers hardness for TiMoTaNbV alloys homogenized at 1300°C for 4 h. Vickers hardness values of the other refractory HEAs were referred for comparison

4. Conclusions

The following results were derived from this study.

1. The determined thermodynamic values of Ω-parameter and δ for the present HEAs were found to be $\Omega \geq 1.1$ and $\delta \leq 6.6\%$ with VEC < 6.87, favoring the HEAs with BCC solid solutions.
2. XRD patterns of the equiatomic $Ti_{20}Mo_{20}Ta_{20}Nb_{20}V_{20}$, and the non-equiatomic $Ti_{40}Mo_{15}Ta_{15}Nb_{15}V_{15}$ and $Ti_{60}Mo_{10}Ta_{10}Nb_{10}V_{10}$ HEAs showed single BCC phases, shifting slightly to the right because of lattice distortion. The lattice parameters of the HEAs estimated using the rule of mixtures were reasonably similar to those of HEAs measured using the XRD analysis.
3. The different solidification rate as a function of melting temperature resulted in the micro-segregation associated with the elements Ta and Mo enriched in the dendrite arms and for the elements V and Ti in the inter-dendritic regions. The micro-segregation in the HEAs was confirmed with the partition coefficient of each alloying element analyzed with the EDS.
4. The HEA specimens showed a decrease in hardness with higher concentration of element Ti because the intrinsic hardness of Ti is lower as compared to the intrinsic hardness of Nb and Mo.

Acknowledgments

This research was supported by the Basic Science Research Program of the National Research Foundation of Korea (NRF) funded by the Ministry of Education (NRF-2018R1D1A1B07041526).

REFERENCES

[1] B. Cantor, I.T.H. Chang, P. Knight, A.J.B. Vincent, Mater. Sci. Eng. A. **375-377**, 213 (2004).

[2] J.W. Yeh, S.K. Chen, S.J. Lin, J.Y. Gan, T.S. Chin, T.T. Shun, C.H. Tsau, S.Y. Chang, Adv. Eng. Mater. **6**, 299 (2004).

[3] G. Mani, Biomater. **28**, 1689 (2007).

[4] S. Sheikh, S. Shafeie, Q. Hu, J. Ahlstrom, C. Persson, J. Veselý, J. Zýka, U. Klement, S. Guo, J. Appl. Phys. **120**, 164902 (2016).

[5] C.C. Juan, K.K. Tseng, W.L. Hsu, M.H. Tsai, C.W. Tsai, C.M. Lin, S.K. Chen, S.J. Lin, J.W. Yeh, Mater. Lett. **175**, 284 (2016)

[6] V. Soni, O.N. Senkov, B. Gwalani, D.B. Miracle, R. Banerjee, Sci. Rep. **8**, 8816 (2018)

[7] O.N Senkov, G.B wilks, D.B. Miracle, C.P Chuang, P.K Liaw, Intermetallics **18**, 1758 (2010).

[8] H.W. Yao, J.W. Qiao, J.A. Hawk, H.F. Zhou, M.W. Chen, M.C. Gao, J. Alloys. Compd. **696**, 1139 (2017).

[9] Y. Zhnag, Z.P. Lu, S.G. Ma, P.K. Liaw, Z. Tang, Y.Q. Cheng, M.C. Gao, MRS Commun. **4**, 57 (2014).

[10] Y. Zahng, Y.J. Zhou, J.P. Lin, G.L. Chen, P.K. Liaw, Adv. Eng. Mater. **10**, 534 (2008)**.**

[11] S. Guo, C. Ng, J. Lu, C.T. Liu, J. Appl. Phys. 109, 103505 (2011).

[12] L. Vegard, Z. Phys. A. At. Nucl. **5**, 17 (1921).

[13] C.C. Juan, M.H. Tsai, C.W. Tsai, C.M. Lin, W.R. Wang, C.C. Yang, S.K. Chen, S.J. Lin, J.W. Yeh, Intermetallics **62**, 76 (2015).

[14] H.W. Yao, J.W. Qiao, M.C. Gao, J.A. Hawk, S.G. Ma, H.F. Zhou, Entropy **18**, 189 (2016).

[15] O.N. Senkov, G.B. Wilks, J.M. Scott, D.B. Miracle, Intermetallics **19**, 698 (2011).

[16] O.N. Senkov, V. Senkova, D.B. Miracle, C. Woodward, Mater. Sci. Eng. A **565** 51 (2013).

[17] E. Fazakas, V. Zadorozhnyy, L.K. Varga, A. Inoue, D.V. Louzguine-Luzgin, F. Tian, L. Vitos, Int. J. Refract. Hard. Met. **47**, 131 (2014).